Application of Artificial Fluid Properties for Stable and Accurate Large-Eddy Simulations of Compressible Turbulent Reactive Flows

H. D. Ranadive[1], H. Wang[1] and E. R. Hawkes[1,2]

[1]School of Mechanical and Manufacturing Engineering
University of New South Wales, NSW 2052, Australia

[2]School of Photovoltaic and Renewable Energy Engineering
University of New South Wales, NSW 2052, Australia

Abstract

In large-eddy simulations (LES) of turbulent reactive flows, typically employed numerical schemes suitable for proper resolution of turbulent structures are not appropriate for capturing steep scalar gradients. In the present work, artificial fluid properties (AFP) have been applied in local regions of sharp scalar variations alongside non-dissipative, explicit central difference schemes to ensure stability without compromising on accuracy. Simulation of a 1D laminar premixed flame using this approach shows that for grids in which there are very few points across the flame, AFP is needed for a stable and accurate flame solution. The dissipation introduced by AFP is verified to be insignificant in the case of a Taylor-Green vortex, in which steep scalar gradients are absent. Finally, a 3D compressible temporal mixing layer is validated by comparing the results from the AFP-based LES with those from dynamic Smagorinsky model-based LES and filtered direct numerical simulation (DNS). Overall, it is shown that the artificial properties provide adequate high wavenumber dissipation enabling stability on coarse grids and compensating for the unresolved sub-grid dissipation. Thus this numerical method is found to be a good candidate for high resolution LES of turbulent flows in which high scalar gradients are present.

Introduction

Numerical simulations of turbulent reactive flows have great utility to improve the prediction and design of combustion devices such as IC engines, gas turbines, and so on. With increasing computational power large-eddy simulations (LES) are now playing an important role in industrial problems [14].

The cut-off scales in LES have significant energy as compared to direct numerical simulations (DNS) and thus discretisation errors can potentially pollute the solution [16]. These inaccuracies can overwhelm the sub-grid dissipation model [13, 17] if numerical methods are not accurate enough. Thus compact or higher order central difference schemes with the non-linear term in skew-symmetric form have been recommended for LES codes [16]. However, for simulations of reactive flows, it is imperative that the numerical method should be dissipative enough to avoid Gibbs oscillations in presence of strong scalar gradients. These two criteria are conflicting, which presents challenges for stable yet accurate LES of compressible reactive flows.

In literature, there have been different numerical schemes used for LES of compressible flows with shocks or large scalar gradients. Jaberi et al. [10] used the compact parameter scheme of Carpenter [2] to stabilise the code with sharp scalar gradients in otherwise high resolution turbulent flows. Alternatively, dissipative mechanisms based on upwind schemes like WENO have been combined with central difference schemes using accurate discontinuity sensors [9]. A post-processing filter algo-

rithm was presented by Yee et al. [18] in which numerical stability at discontinuities was achieved using dissipative portion of a shock-capturing scheme with a local flow sensor. In hybrid central-upwind schemes as discussed above, the expensive computations of characteristic-based upwind schemes might be active only in few of the parallel processors causing inefficient computational load distribution.

A novel approach was proposed by Cook [4] in which a high wavenumber (artificial) viscosity was used to provide a sharp cut-off near the Nyquist wavenumber ($\pi/\Delta x$) and hence implicitly provide sub-grid dissipation, rather than modelling the unclosed terms obtained in filtered governing equations. This was later extended to handling thermal and material discontinuities in high resolution turbulent flows [4, 5]. The artificial properties were evaluated in the entire flow field but were computationally less expensive than characteristic-based upwind schemes. This algorithm has been assessed and validated for shock-turbulence interaction [4, 11] and in supersonic combustion problems [5]. However, the possibility of applying this method of artificial properties has not been tested for subsonic LES of reactive flow problems in literature so far.

In this paper, we apply the artificial fluid properties (AFP) approach in the context of LES to various reactive and non-reactive flow configurations. We first verify the stabilisation capability of AFP scheme on coarse grids (demonstrated using a laminar premixed 1D flame), then assess the dissipation of turbulent structures without strong scalar gradients (3D inviscid Taylor-Green vortex); finally we test the capability of artificial viscosity as a sub-grid model for LES (3D temporal mixing layer). The remainder of the paper is organised as follows. The next section discusses the numerical methodology including the details about the AFP approach. The section on results and discussion follows, including the configuration details and relevant analysis. Finally concluding remarks are drawn.

Numerical Scheme

Fully compressible system of equations conserving momentum, energy and species mass fractions are solved using a MPI-based Fortran code, S3D [3]. The viscous stresses are evaluated assuming Newtonian fluid properties while the heat and mass diffusion fluxes are evaluated using the Fourier and Fick's laws respectively.

The system of equations are integrated in time using a six stage and fourth order accurate explicit Runge-Kutta algorithm. The first derivatives are calculated using sixth order central difference scheme. High frequency solution components are suppressed using filtering techniques. Both explicit [12] and compact [8] filters have been implemented in the code. The system of equations resulting in a compact filter were solved using an external library PETSc [1].

The fluid properties like shear viscosity (μ), mass diffusivity (D_i) and thermal conductivity (λ) are modified in the AFP implementation by adding their respective artificial contributions. The expressions for these artificial properties are as follows [4]:

$$\mu^* = C_\mu \overline{\rho \mid \nabla^r S \mid} \Delta^{(r+2)}, \tag{1}$$

$$\lambda^* = C_\lambda \overline{\frac{\rho c_s}{T} \mid \nabla^r e \mid} \Delta^{(r+2)}, and \tag{2}$$

$$D_i^* = C_D \overline{\mid \nabla^r Y_i \mid} \frac{\Delta^{(r+2)}}{\Delta t} \tag{3}$$

where $S = \sqrt{\mathbf{S.S}}$ is the magnitude of the strain rate tensor, $\Delta = (\Delta x \Delta y \Delta z)^{1/3}$ is the local grid spacing, T is the temperature, ρ is the density, c_s is the speed of sound, Y_i is the ith species mass fraction, Δt is the time step and e is the internal energy.

The operator ∇^r denotes a higher derivative (r taken as 4 in this implementation) and the overbar denotes an approximate truncated Gaussian filter (of filter size 4Δ) [4] to smooth out the higher derivatives. C_μ, C_λ and C_D are constants whose values are taken as 0.002, 0.01 and 0.003 respectively [4] except in the 1D laminar premixed flame case wherein the constants are taken as 0.02, 0.1 and 0.03 to stabilise the sharp discontinuity arising at the flame front, which spreads across 3-4 grid points only in the coarsest grid used. Artificial bulk viscosity [4] is not included in this implementation because we consider flows without significant compressibility or shock waves.

Results and Discussion

1D Laminar Premixed Flame

A stoichiometric methane-air flame is initialised with premixed reactants at 300 K (T_u) on one side and products at 2259 K (adiabatic flame temperature) on the other side. The computational domain is one dimensional (1D) having length of 20 mm. A reduced 2-step methane mechanism comprising of 6 species was used to model chemistry. The equilibrium equations are $CH_4 + 1.5O_2 \rightleftharpoons CO + 2H_2O$ and $CO + 0.5O_2 \rightleftharpoons CO_2$ [7].

A reference case was obtained using a fine grid ($\Delta x = 20\ \mu$m), which resolves all of the flame structures. The flame thickness ($\delta = 640\ \mu$m) and flame speed ($S_L = 0.4$ m/s) from the reference case are compared with the results obtained using coarser grids.

Nx	Δx (μm)	δ/Δx
1024	20	31.8
320	62.5	10.2
200	100	6.4
120	167	3.8

Table 1: Summary of grids used for the 1D laminar flame test

The steady solutions for different grid sizes are shown in Figure 1. AFP along with a compact filter were utilised in all cases shown in Figure 1, except the reference case. It is seen that with increasing grid size, the flame becomes thicker, which is consistent with the fact that the scalar profile becomes wider when applying a larger filter size to the laminar flame. For fine grids the solution converges to that of the reference case.

The fuel consumption rate ($\dot{\omega}_F$) is integrated over the domain to evaluate the laminar flame speed as follows:

$$S_L = \frac{-\int_{-\infty}^{\infty} \dot{\omega}_F dx}{\rho_u Y_{F,u}}, \tag{4}$$

where ρ_u is the density of the un-burnt reactants and $Y_{F,u}$ is the fuel mass fraction in the reactant species.
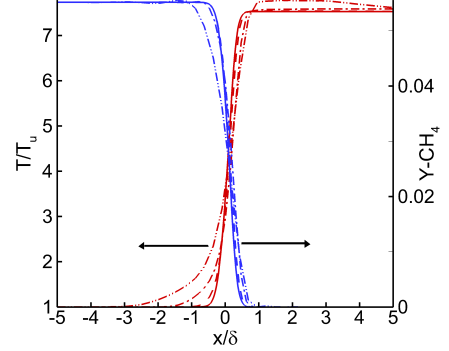

Figure 1: Temperature (red) and methane mass fraction (blue): 1024 points (solid line); 320 points (dashed line); 200 points (dashed-dot line); and 120 points (dashed-dot-dot line)

The error in evaluating flame speeds with respect to the reference case is shown in Figure 2 for different numerical methods. It should be noted that the explicit filter was incapable of removing high frequency components in the coarsest grid and the simulation crashed. Compact filtering along with artificial properties enabled more accurate flame predictions on coarse meshes due to its selective damping of high frequency numerical oscillations. With the resolution of 167 μm, the error in the flame speed using the compact filter and artificial properties is about 6%, compared with 12% without artificial properties.
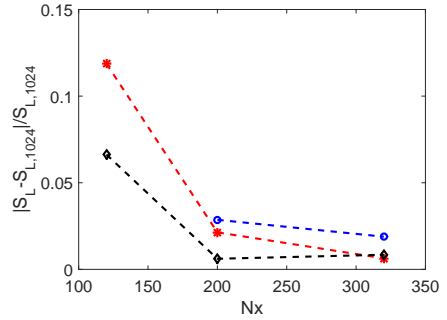

Figure 2: Error in flame speed: compact-AFP (Black $\diamond$); compact without AFP (Red $*$); and explicit without AFP (Blue $\circ$)

3D Inviscid Taylor-Green Vortex

The ability of the numerical method to resolve small-scale turbulence is evaluated using an inviscid Taylor-Green vortex configuration. A periodic box of dimension $[0, 2\pi]$ having 64^3 grid points is initialised with well resolved and smooth properties. The complete details about the initialisation are available in [4] and not repeated here for the sake of brevity. As the time is advanced, the turbulent cascade generates smaller structures with no lower limit on the length scale [11].

The simulation using the compact filter, with and without artificial properties, successfully conserves the kinetic energy as seen from Figure 3a. At later time stages (after t=4), the kinetic energy drops when the scales of motion become unresolvable for the available grid spacing. It is noted that AFP does not cause a significant degradation or dissipation of the turbulent flow scales.

The enstrophy is observed to increase rapidly as small-scale turbulence develops before reaching a maximum value. It is observed from Figure 3b, that the trends with and without AFP

(a) Turbulent kinetic energy
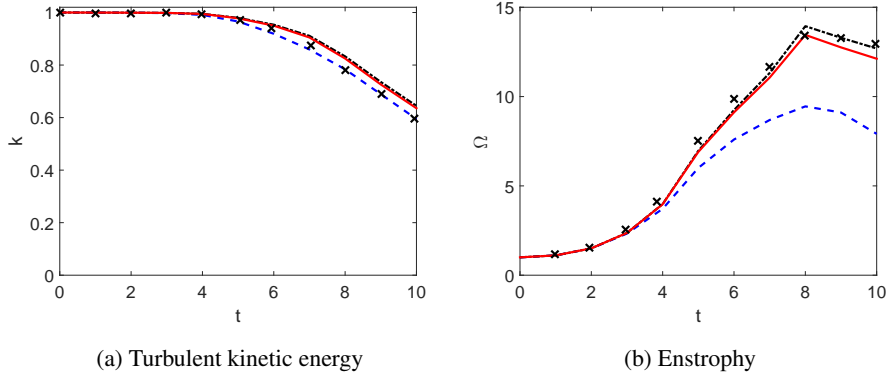

(b) Enstrophy

Figure 3: Comparison of turbulent kinetic energy and enstrophy for Taylor-Green vortex: compact (black dashed dotted line); compact + AFP (red solid line), explicit (blue dashed line); and Cook [4]: compact + AFP (symbols ×)

(using the compact filter) do not differ significantly. Explicit filtering of high frequency components causes significant dissipation and does not allow the smallest length scales (possible on the grid) to develop. Finally, the profiles obtained using compact filter (with and without AFP) match favourably with those presented by Cook [4] who used the AFP approach along with compact finite difference schemes and compact filters.

3D Temporal Mixing Layer

In this section, both DNS and LES of a 3D mixing layer are performed to further explore the ability of the AFP scheme to serve as a sub-grid model for LES. The configuration involves two streams composed of air having different velocities ($U_1 = -U_2$) but equal temperature and pressure. A convective Mach number (defined as $M_c = (U_1 - U_2)/(c_1 + c_2)$, c_1 and c_2 being the speed of sound in streams 1 and 2 respectively) of 0.3 was used in this simulation. The vorticity thickness (δ_ω) and velocity difference ($\Delta U = U_1 - U_2$) are used to define the Reynolds number. The initial momentum thickness ($\delta_{\theta 0}$) = 0.0109 mm and $Re = 705$ were used as in [6, 15]. Isotropic turbulence is first generated using Passot-Pouquet energy spectrum having a turbulent intensity equal to 10% of U_1 and an integral length scale of 0.62 mm. The initial streamwise velocity profile and the shape function to limit the initial turbulence to the shear layer have been used as in [6]. Periodic boundary conditions are used in both streamwise (x) and spanwise (z) directions while non-reflecting boundary conditions were applied in the normal (y) directions.

Table 2 gives a summary of the non-dimensional domain extents and grid points used for both the DNS and LES simulations. The DNS grid was set to be 3.5 times the minimum Kolmogorov scale encountered during the temporal evolution of the mixing layer. The same LES grid was used for both the AFP and the dynamic Smagorinsky (DS) model-based simulations. The compact filter was used to damp high frequency oscillations. However, as the there are no scalar gradients in this configuration, only the artificial viscosity is relevant for the simulations.

	$Lx/\delta_{\theta 0}$	$Ly/\delta_{\theta 0}$	$Lz/\delta_{\theta 0}$	Nx	Ny	Nz
DNS	1032	387	172	1536	576	256
LES	1032	387	172	464	240	64

Table 2: Domain and grid used for the temporal mixing layer

Figure 4 shows the growth of momentum thickness (δ_θ) with time. As reported in previous references [6, 15] we observe a linear increase in δ_θ after an initial transient. The LES simu-

lations based on both AFP and DS exhibit trends similar to the filtered DNS results, that were obtained by applying a box filter with a filter size of 4 times the DNS grid spacing. The final Re attained in this simulation was approximately 20000.
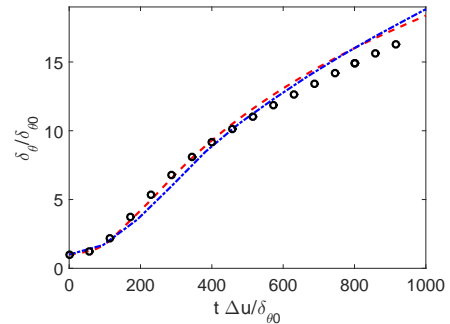

Figure 4: Growth of momentum thickness: AFP (red dashed line), dynamic Smagorinsky (blue dashed-dot line) and filtered DNS (symbols o)

The turbulent stress tensor (based on Favre fluctuations) is calculated as [6],

$$R_{ij} = \frac{\left\langle \rho u_i'' u_j'' \right\rangle}{\langle \rho \rangle} \qquad (5)$$

Self-similar profiles of R_{11} and R_{12} are shown in Figure 5. The normal coordinate has been non-dimensionalised with the time varying vorticity thickness ($\delta_\omega(t)$). As expected in the fully developed turbulent stage, the profiles collapse into a self-similar regime. Apart from a slight over-prediction of peak turbulent intensities, the AFP-based LES plots are in reasonable agreement with the filtered DNS results.

Conclusions

Numerical schemes form a critical component in LES of turbulent reactive flows. On the one hand, the numerical dissipation should be minimal for accurate resolution of turbulent structures, while on the other hand the scheme should be stable enough to capture scalar gradients on coarse grids that are typically used in LES. In this work, we have explored the application of artificial properties alongside non-dissipative central difference schemes to address the aforementioned challenge. The test cases presented have been selected to verify separately the capability of the algorithm to stabilise steep scalar gradients, resolve high resolution turbulence and compensate for sub-grid
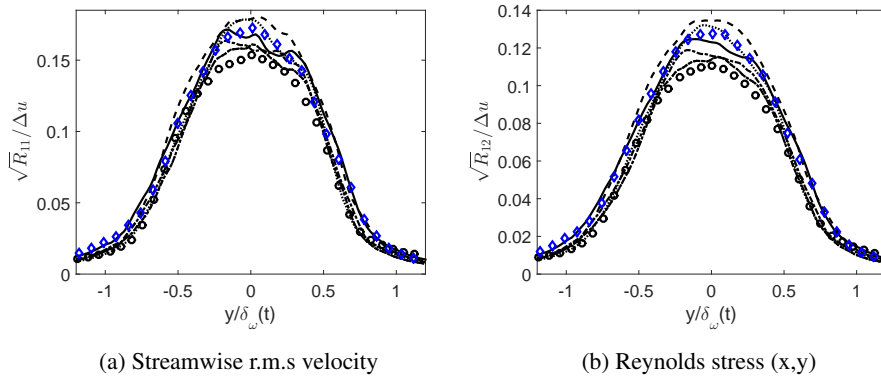
(a) Streamwise r.m.s velocity   (b) Reynolds stress (x,y)

Figure 5: Turbulent intensities for AFP-LES: t=572 (dashed line), t=667 (dotted line), t=763 (solid line), t=858 (dashed-dotted line) and t=954 (solid line with circular markers); dynamic Smagorinsky LES at t=763 (blue ◇); and filtered DNS at t=763 (black ○)

scale dissipation. The long term goal of this research is to develop a very accurate and stable LES solver for compressible turbulent reactive flows.

Acknowledgements

References

[1] Balay, S., Abhyankar, S., Adams, M., Brown, J., Brune, P., Buschelman, K., Dalcin, L., Eijkhout, V., Gropp, W., Kaushik, D., Knepley, M., McInnes, L. C., Rupp, K., Smith, B., Zampini, S., Zhang, H. and Zhang, H., PETSc users manual, Technical Report ANL-95/11 - Revision 3.7, Argonne National Laboratory, 2016.

[2] Carpenter, M. H., A high-order compact numerical algorithm for supersonic flows, *Twelfth International Conference on Numerical Methods in Fluid Dynamics*, 254–258.

[3] Chen, J. H., Choudhary, A., De Supinski, B., DeVries, M., Hawkes, E. R., Klasky, S., Liao, W. K., Ma, K. L., Mellor-Crummey, J., Podhorszki, N., Sankaran, R., Shende, S. and Yoo, C. S., Terascale direct numerical simulations of turbulent combustion using S3D, *Computational Science and Discovery*, **2**, 2009, 1–31.

[4] Cook, A. W., Artificial fluid properties for large-eddy simulation of compressible turbulent mixing, *Physics of Fluids*, **19**, 2007, 1–9.

[5] Fiorina, B. and Lele, S. K., An artificial nonlinear diffusivity method for supersonic reacting flows with shocks, *Journal of Computational Physics*, **222**, 2007, 246–264.

[6] Foysi, H. and Sarkar, S., The compressible mixing layer: an LES study, *Theoretical and Computational Fluid Dynamics*, **24**, 2010, 565–588.

[7] Franzelli, B., Riber, E., Gicquel, L. Y. M. and Poinsot, T., Large-eddy simulation of combustion instabilities in a lean partially premixed swirled flame, *Combustion and Flame*, **159**, 2012, 621–637.

[8] Gaitonde, D. V. and Visbal, M. R., Pade-type higher-order boundary filters for the Navier-Stokes equations, *AIAA Journal*, **38**, 2000, 2103–2112.

[9] Hill, D. J. and Pullin, D. I., Hybrid tuned center-difference-WENO method for large-eddy simulations in the presence of strong shocks, *Journal of Computational Physics*, **194**, 2004, 435–450.

[10] Jaberi, F. A., Colucci, P. J., James, S., Givi, P. and Pope, S. B., Filtered mass density function for large-eddy simulation of turbulent reacting flows, *Journal of Fluid Mechanics*, **401**, 1999, 85–121.

[11] Johnsen, E., Larsson, J., Bhagatwala, A. V., Cabot, W. H., Moin, P., Olson, B. J., Rawat, P. S., Shankar, S. K., Sjogreen, B., Yee, H. C., Zhong, X. and Lele, S. K., Assessment of high-resolution methods for numerical simulations of compressible turbulence with shock waves, *Journal of Computational Physics*, **229**, 2010, 1213–1237.

[12] Kennedy, C. A. and Carpenter, M. H., Several new numerical methods for compressible shear-layer simulations, *Applied Numerical Mathematics*, **14**, 1994, 397–433.

[13] Kravchenko, A. G. and Moin, P., On the effect of numerical errors in large-eddy simulations of turbulent flows, *Journal of Computational Physics*, **131**, 1997, 310–322.

[14] Lacaze, G., Cuenot, B., Poinsot, T. and Oschwald, M., Large-eddy simulation of laser ignition and compressible reacting flow in a rocket-like configuration, *Combustion and Flame*, **156**, 2009, 1166–1180.

[15] Pantano, C. and Sarkar, S., A study of compressibility effects in the high-speed turbulent shear layer using direct simulation, *Journal of Fluid Mechanics*, **451**, 2002, 329–371.

[16] Park, N., Yoo, J. Y. and Choi, H., Discretization errors in large-eddy simulation: on the suitability of centered and upwind-biased compact difference schemes, *Journal of Computational Physics*, **198**, 2004, 580–616.

[17] Vreman, B., Geurts, B. J. and Kuerten, H., Comparison of numerical schemes in large-eddy simulation of the temporal mixing layer, *International Journal for Numerical Methods in Fluids*, **22**, 1996, 297–311.

[18] Yee, H. C., Sandham, N. D. and Djomehri, M. J., Low-dissipative high-order shock-capturing methods using characteristic-based filters, *Journal of Computational Physics*, **150**, 1999, 199–238.